Cite this article
Prabhakaran M, Jeyasimman D and Varatharajulu M
Investigation of the failure mechanism of dissimilar resistance spot welding of steels.
Emerging Materials Research,
https://doi.org/10.1680/jemmr.22.00224

Research Article
Paper 2200224
Received 13/12/2022; Accepted 04/04/2023
First published online 11/04/2023

Emerging Materials Research

ice Publishing

Investigation of the failure mechanism of dissimilar resistance spot welding of steels

M. Prabhakaran
Research Scholar, Department of Mechanical Engineering, Periyar Maniammai Institute of Science and Technology, Thanjavur, India; Assistant Professor, Department of Mechanical Engineering, Agnel Institute of Technology and Design, Bardez, India

D. Jeyasimman
Professor, Department of Mechanical Engineering, Periyar Maniammai Institute of Science and Technology, Thanjavur, India (corresponding author: jeyasimman76@gmail.com; jeyasimmand@pmu.edu)

M. Varatharajulu
Associate Professor, Department of Mechanical Engineering, Sri Krishna College of Technology, Kovaipudur, India

Austenitic and duplex stainless steels are majorly preferred for heat exchangers and chemical containers. This research work investigated the failure mechanism of dissimilar welded joints of AISI 347 and DSS 2205. The welded specimens were investigated using tensile shear tests, cross-tension tests, coach peel tests and microhardness tests. The specimen absorbed a maximum tensile shear load of 18 kN during the tensile shear test, and the failure mode was button pull-out with brittle fracture. The test sample absorbed a load of 15.1 kN during the cross-tension test, and the failure mode was button pull-out with brittle fracture. During the coach peel test, the sample absorbed a maximum load of 4 kN and ductile fracture was observed at the vicinity of the nugget. The failure mode in the coach peel test was of button pull-out type. The microhardness test recorded a maximum hardness of 312.8 HV, which is 78.74 and 7.1% higher than the base metal hardness values of AISI 347 and AISI 2205, respectively. The specimen failed under pull-out failure mode in all the tests, and hence, the weld zone was intact in all specimen arrangements and loading conditions.

Keywords: AISI 347/coach peel test/cross-tension test/DSS 2205/material characterisation/material properties/microhardness test/tensile shear test

1. Introduction

The joining of metal sheets using resistance spot welding (RSW) has gained wide popularity over the past few decades. In particular, automotive body-in-white and aerospace applications are highly reliant on the RSW process for the aesthetics of the vehicle body and the strength of the load-bearing structures. The simple arrangement of the RSW mechanism and its versatility in welding a wide range of materials makes RSW a reliable and quick way of joining sheet metals. The relatively cheaper and repeatable nature of RSW is the most sought factor in the industrial usage of this process. Although the metal-joining process plays a significant role in the strength of the fabrication process, the material used should be given true credit. The advancement in materials technology has given rise to application-specific materials with special surface treatments. Stainless steels in particular have evolved to a greater extent for harsh environment applications. In this regard, duplex stainless steels (DSSs) have proven themselves as materials with high potential for corrosion resistance and low-weight-high-strength applications. The unique behaviour of DSS makes it very much apt for the crumple zone of automobiles.[1–3]

Chen *et al.*[4] studied the effect of the welding parameters, welding time and welding current on the shear strength of the weld nugget in RSW of low-carbon (C) steel and stainless-steel plates. Chabok *et al.*[5] performed an innovative study of the RSW of third-generation advanced high-strength steel (AHSS) by heat-treating welded samples as similarly done in the paint-baking process of automobiles and performed a bending test by creating micro-cantilevers on the weld specimen. In a work carried out by Ding *et al.*,[6] investigations were done on the RSW of twinning-induced plasticity (TWIP) steel in normal mode and microstructure manipulation mode by introducing interlayer foils between the steel sheets. The strength of the weld nugget formed with interlayer foils increased significantly relative to that for the normal mode. Rao *et al.*[7] performed RSW of DP590 steel sheets and optimised the parameters using a hybrid RSM–genetic algorithm method. Zhao *et al.*[8] researched on improving the cross-tension properties of AHSS by optimising the welding parameters. Mishra *et al.*[9] researched the RSW of different combinations of mild steel and stainless steel, and optimisation of the parameters was done using the desirability approach. In a similar work done by Zhang *et al.*,[10] dissimilar welds of ferritic 430 stainless steel and austenitic 304 stainless steel were made under all possible combinations, and it was concluded that the 430/304 combination possesses greater hardness and toughness than the other combinations. Prabhakaran *et al.*[11] investigated dissimilar spot welding of austenitic stainless steel and DSS, wherein the macrographs and scanning electron microscopy (SEM) images of the welded region were used to investigate thoroughly its microstructure and failure mode during a tensile shear test (TST). In a critical research work done by Shojaee *et al.*,[12] AHSSs of two different grades were spot-welded separately and TSTs and cross-tensile tests (CTTs) were done on the samples. The results showed that the failure mode had no correlation with the weld strength, and hence, the type of failure was not a better criterion for judging the weld performance. In the authors' earlier studies, the effect of intermetallic compounds and

inclusions in carbon–manganese (Mn) steel plate butt joint welding failure,[13] and the influence of the welding sequence on residual stresses induced in the as-welded plug weld of low-carbon steel[14] was investigated. Pandya *et al.*[15] performed a modified CTT and a coach peel test (CPT) to study the fracture response of dual-phase steel sheets by using a customised testing apparatus. A finite-element model study of the CPT was carried out to predict the property change in different zones of the weld, and the results were validated with the actual experiments.[16] The researchers considered the low voltage requirement and environmentally clean nature of RSW as the prime reasons for preferring RSW. There were no available data to make a comparative study on the CPT, cross-tension test and the microhardness test of dissimilar welding of AISI 347 and AISI 2205 grades of stainless steel. This lack of data formed the basis of the current research work, wherein the mechanical properties of a dissimilar weld were investigated under various testing conditions.

2. Experimental methodology

This research work focuses on analysing the weld characteristics of dissimilar spot welding of AISI 347 stainless steel and DSS 2205. The chemical compositions and the mechanical properties of the base metals are given in Tables 1 and 2, respectively. The principle of RSW is shown in S1 in the online supplementary material. The weld trials were carried out in a microprocessor-controlled manual-pedal-operated Nash 815 V2 RSW machine. The layout and dimensions of the welded specimens are shown in Figure 1.

The welded specimens were then cut along the nugget using a wire-cut electric discharge machine to expose the nugget area for inspection. The exposed surface was macro-etched in accordance with the standard procedure to carry out the macrograph studies.

The TST was carried out by using a Tinius Olsen H50KL TST machine at a loading rate of 1 mm/min, for all the welded samples. A schematic diagram of the TST is shown in S2 in the online supplementary material. The parameters used for the RSW process are shown in Table 3. Samples 6 and 9, which failed under the maximum load in the TST, were welded again with the same set of parameters for carrying out the CPT, CTT and microhardness test. The CTT and CPT were carried out using the TST machine. Schematic diagrams of the CPT and CTT are shown in S3 and S4 in the online supplementary material, respectively. The microhardness test was done using Struers Duramin-4M1 testing apparatus with a loading of 500 gram-force (gf) and a dwell time of 15 s. The hardness of the weld nugget was tested across its length and width.

Table 2. Mechanical properties of AISI 347 and DSS 2205

Property	Unit	AISI 347	DSS 2205
Yield strength (0.2%)	MPa	205	448
Tensile strength	MPa	525	621
Elongation	%	34	25
Hardness	HV	175	292
Elasticity	GPa	201	190
Density	kg/m^3	8000	7800

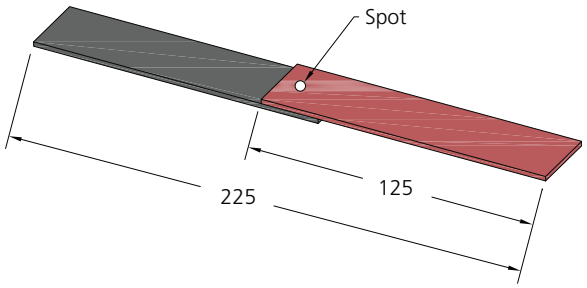

Figure 1. RSW specimen (all dimensions in mm)

Nine various specimens were welded with two variable welding parameters and three constant parameters. The squeezing time and holding time were held constant at 50 cycles and ten cycles, respectively, and the electrode tip diameter was kept constant at 10 mm. The welding current and heating time cycles were varied in RSW, as shown in Table 3. After the spot welding had been done, all the samples were wire-cut to expose and investigate the weld nugget. A macroscopic examination was carried out on all the specimens, but the weld nuggets of samples 6 and 9 were found without any defects, as shown in S5 in the online supplementary material.

3. Results and discussion

3.1 Failure mode analysis of the TST

In the TST, nine samples were tested, and the tensile shear characteristics of the welded specimens could be inferred by studying the load–displacement curves shown in Figure 2. The results show that sample 9, followed by sample 6, absorbed the

Table 1. Chemical compositions of AISI 347 and DSS 2205

Name of the element	Carbon	Manganese	Silicon (Si)	Chromium (Cr)	Phosphorus (P)	Nickel (Ni)	Sulfur (S)	Niobium (Nb)	Iron (Fe)
AISI 347 composition: %	0.08	2.00	0.75	19.0	0.045	0.02	0.03	1	Rest
DSS 2205 composition: %	0.02	0.82	0.36	22.3	0.030	5.46	0.01	—	Rest

This table was reproduced with permission from the publishers of the paper by Prabhakaran *et al.*[10]

Table 3. Various parameters of the welded specimens

Trial number	1	2	3	4	5	6	7	8	9
Welding current: kA	6.5	6.5	6.5	7.5	7.5	7.5	8.5	8.5	8.5
Heating time (cycles)	10	12	14	10	12	14	10	12	14

This table was reproduced with permission from the publishers of the paper by Prabhakaran *et al.*[10]

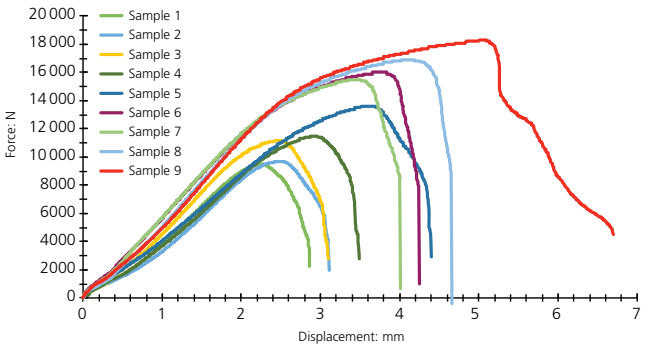

Figure 2. Load–displacement curve of the TST. This figure was reproduced with permission from the publishers of the paper by Prabhakaran *et al.*[11]

maximum shear load before failure. Samples 9 and 6 failed after withstanding tensile forces of 18 and 16 kN, respectively. The investigation of the tensile-shear-failed samples showed that all the samples except one failed under interfacial mode and sample 9 failed under button pull-out failure mode. A similar inference has been obtained for dissimilar RSW of TWIP steel with austenitic stainless steel.[17] However, in a study of dissimilar welding of austenitic SS 316 and titanium alloy by Taufiqurrahman *et al.*,[18] wherein the welding current ranged between 11.0 and 13.0 kA, all the samples failed under interfacial mode during the TST. This reveals that the failure mode is not purely dependent on the welding current and nugget size but is also dependent on the metallurgy of the parent metals. The current research also reinforces the fact that an austenitic stainless-steel specimen welded with a welding current above 7.5 kA results in pull-out failure mode.

During the TST of sample 9, the nugget was completely detached from the lower surface and the nugget on the upper surface can be seen to have undergone substantial plastic deformation before failure, and this shows the possibility of ductile failure. DSS 2205 and AISI 347 formed the lower and upper surfaces of the test specimen. To have an unquestionable conclusion regarding the failure mechanism of the sample under TST, the fractography images shown in Figures 3 and 4 were analysed. Figures 3 and 4 show the fractography images at different magnification levels of the fractured lower and upper surfaces, respectively, of sample 9. The fractography images in Figures 3(a) and 3(b) show the formation of dimples on one side of the scanned region, which is an indication of ductile failure. However, there are clear indications of formation of quasi-cleavages on other side of the scanned region, which also gives the possibility of brittle failure in the weld sample. The fractography images of the upper side of the failed sample in Figures 4(a)–4(d) show clear formation of cleavages. Cleavage formation can be seen evidently at various levels of magnification. This is a demonstrable sign of brittle fracture on the sample. The plastic deformation that occurred in the upper side of the failed sample cannot be also overruled. Now, from a comparison with the fractography images and the mechanical properties of the base metals, the actual failure mechanism of the sample can be drawn. Any ductile failure mechanism will always be associated with necking as a result of reduction in the cross-sectional area of the failure zone. There is no necking phenomenon, and the weld nugget is found to remain intact and the failure mode is button pull-out failure as stated earlier. The failure of the sample initiated from the AISI 347 side with plastic deformation. Since AISI 347 is relatively softer than DSS 2205, it underwent sufficient deformation. However, after absorbing a considerable amount of shear load, a crack initiated on the DSS 2205 base metal at the circumference of the nugget, and upon further loading, the crack propagated around the circumference of the nugget, thereby separating the nugget completely from the lower side of the sample. This argument can be substantiated by comparing the fractography images of the upper and lower sides of the sample. The fractography images in Figure 3 show signs of partial plastic-deformation-assisted ductile failure along with formation of cleavages. The fractography images in Figure 4 show that the detached nugget consists of the remains of DSS 2205, and cleavages are found to be formed in the scanned region. This finally gives a clear conclusion that the failure initiation occurred through ductile mode; however, the final fracture occurred in brittle mode along the circumference of the nugget, thus resulting in a button pull-out failure mode. The results of the trial conducted by Wang *et al.*[19] also observed a considerable increase in the tensile shear strength due to plastic deformation. The load–displacement curve of the TST shown in Figure 2 for sample 9 also agrees with the above inference wherein the strain rate is linear up to 18 kN and then the sample suddenly starts failing beyond that point.

3.2 Failure mode analysis of the CTT

The maximum load absorbed by the specimen before failure is an important parameter in assessing its mechanical properties.[20] A CTT was performed on samples 6 and 9. S6 in the online supplementary material shows the schematic arrangement of the sample for performing a CTT. Holes were drilled on either end of the sheet metal samples to accommodate them on a customised

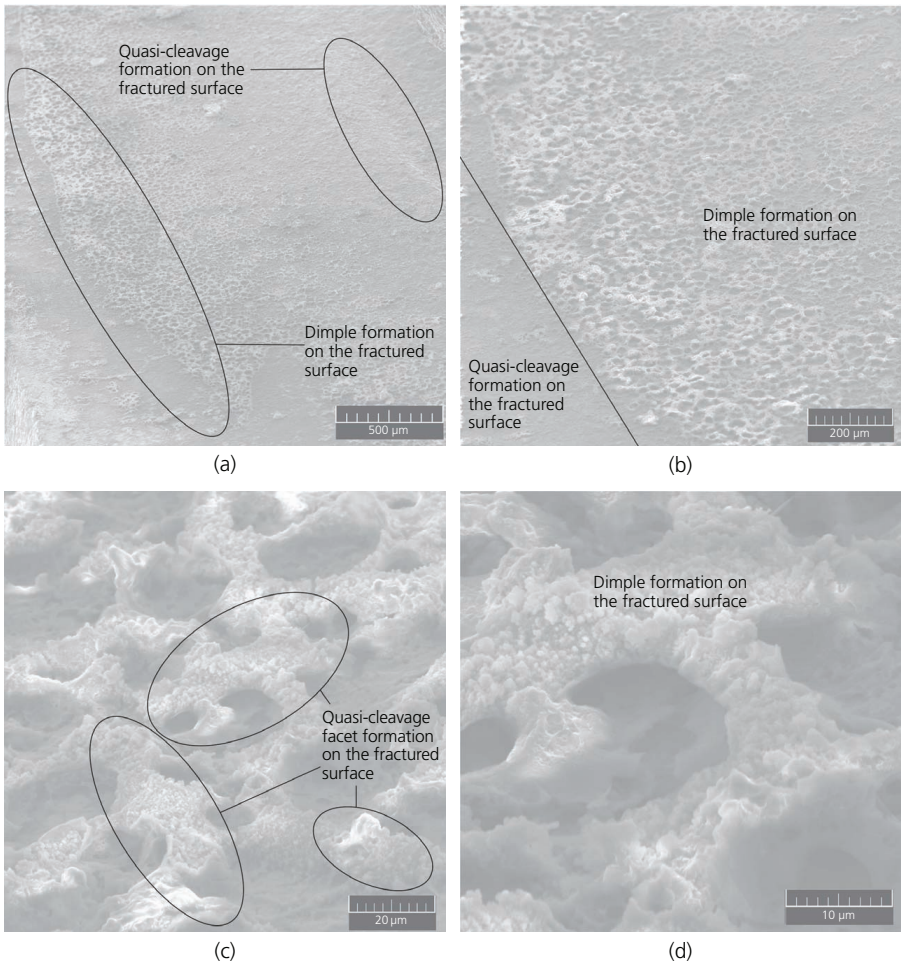

Figure 3. Fractography images of the lower side of sample 9: (a) formation of dimples and quasi-cleavages; (b) dimple formation representing ductile deformation; (c) enlarged view of quasi-cleavage facets representing brittle fracture; (d) enlarged view of partial dimple formation

fixture shown in S7 in the online supplementary material. This fixture in turn was mounted on the Tinius Olsen H50KL tensile-testing machine shown in S8 in the online supplementary material to carry out the CTT. The failed samples of the test are shown in Figures 5 and 6.

The peak load absorbed increases with an increase in the welding current, which subsequently leads to an increase in the weld nugget.[21,22] This inference is confirmed, as sample 9, which was welded with a higher welding current, absorbed at a maximum force of 15.1 kN before failure, which is higher than the failure load of sample 6. The fixture arrangement of the CTT enables the entire tensile load to act directly on the weld nugget unlike that in the TST, wherein the tensile shear load initially acts on the base metal and then gradually brings the nugget into picture. Hence, unlike in the TST, no plastic deformation can be seen on the nugget due to the loading arrangement. The fractography images shown in Figure 7 and the force–displacement curves shown in Figure 8 provide sufficient information for analysing the failure mechanism of the samples during the CTT. In sample 6, the crack initiated from the nugget and then propagated around the circumference, resulted in a partial pull-out failure. As seen in Figure 5, the weld nugget is not fully separated and there are evident signs of fracture through the nugget area. The fractography images shown in Figures 7(a) and 7(b) show the upper and lower surfaces of fractured sample 6. The SEM images of the fractured surface show the formation of cleavage facets, and thus, the fracture mode is found to be brittle. Reinforcing the same inference, the load–displacement curve of sample 6 in Figure 8 also shows the failure mode as brittle. This also agrees with the results obtained by Marashi *et al.*[23] that nuggets with a diameter smaller than the critical value of $4t^{1/2}$ fail through interfacial mode only. Upon investigation of the failure mechanism of sample 9, Figure 6 shows a complete separation of the nugget from its counterpart, which means the failure mode is button pull-out. The fractography images in Figures 7(c) and 7(d) show upper and lower surfaces of the fractured surfaces of sample 9, and the presence of cleavage facets on the lower surface is a

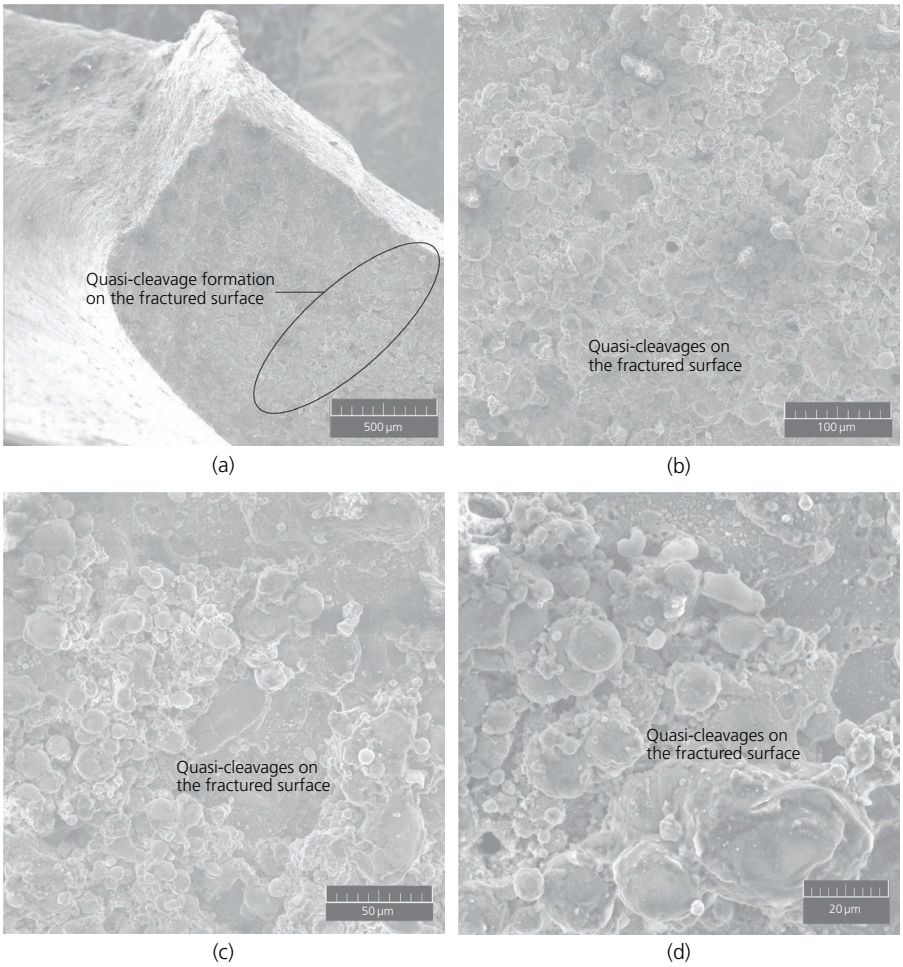

Figure 4. Fractography images of: (a) formation of quasi-cleavage formation on sample 9 upper side; (b) quasi-cleavage formation representing brittle fracture on sample 9 lower side; (c, d) enlarged view of quasi-cleavage formation on sample 9 upper side

Figure 5. CTT-failed sample 6

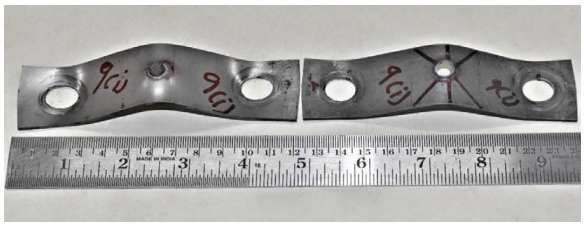

Figure 6. CTT-failed sample 9

clear indication of brittle failure, which is quite natural in the case of pull-out failure. Moreover, according to the literature. the nugget diameter of sample 9 is also clearly above the critical nugget diameter, which will eventually result in pull-out failure.[23]

3.3 Failure mode analysis of the CPT

The specimen configuration for the CPT is shown in S9 in the online supplementary material. A CPT was conducted on samples 6 and 9. The CPT arrangement is shown in S10 in the online supplementary material. The ultimate forces absorbed by samples 6 and 9 during the test were 3.6 and 4 kN, respectively. The peak load absorbed in the CPT increased with the increasing welding current and heating cycles.[21] The ruggedness of an automobile or any welded structure was purely reliant on the strength of the weld, and during the dynamic conditions of the structure, the load would be absorbed by the weld spots predominantly. Hence, it is very critical to ensure that the weld joints do not fail during the dynamic condition for any type of specimen arrangement. S11 in

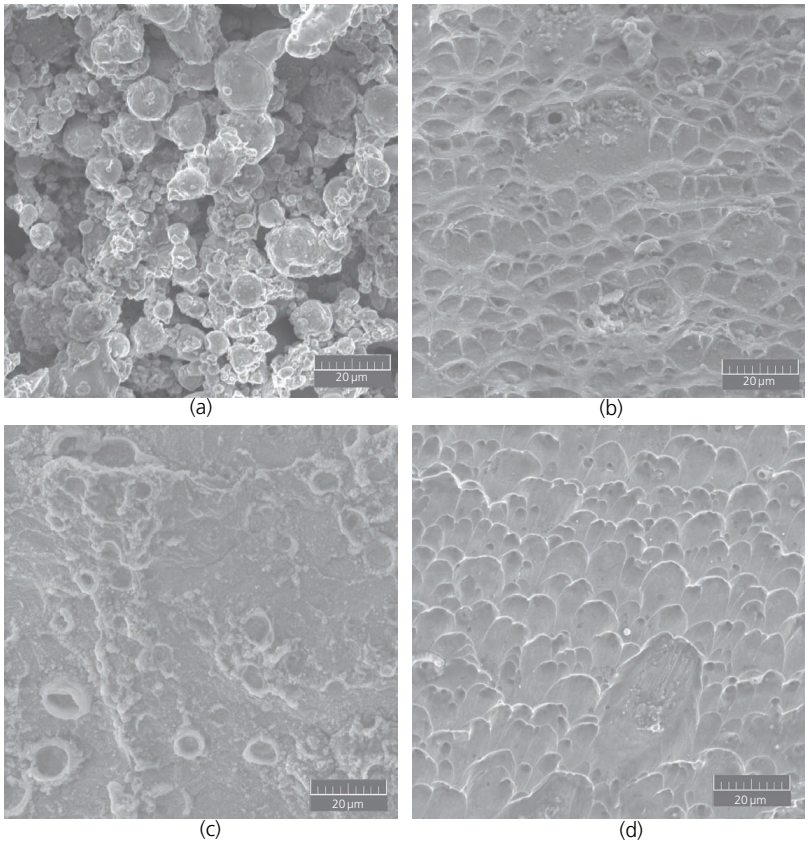

Figure 7. Fractography images of CTT-failed: (a) quasi-cleavage formation in upper side of fractured sample 6; (b) brittle fracture representation of lower side of fractured sample 6; (c) dimple formation on upper side of fractured sample 9; (d) quasi-cleavage formation in upper side of fractured sample 9

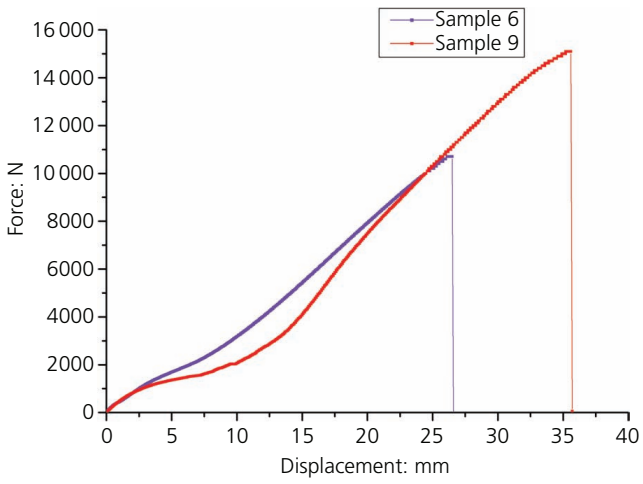

Figure 8. Load–displacement curve of the CTT

the online supplementary material shows the failed specimens of samples 6 and 9 during the CPT, where it can be seen that the specimens underwent complete button pull-out failure with a considerable tear in the parent metal only. Arumugam and Pramanik[24] in a dissimilar RSW work also encountered a similar way of pull-out failure mode of samples during the CPT. The fractography images of the failed samples in Figure 9 show the formation of an array of dimples, which is a proper depiction of ductile failure. The load–displacement curves of samples 6 and 9 in Figure 10 also show proper ductile failure of both specimens with substantial plastic deformation. The weld nugget is completely intact, and tearing is noticed in AISI 347, as it is softer than DSS 2205. This proves that the weld parameters for sample 9 is the best combination, as the weld nugget did not fail in the CTT and CPT.

3.4 Analysis of microhardness test results

The hardness was measured using a Vickers hardness tester equipped with a diamond pyramid, as specified by ASTM E 384.[25] Microhardness (VHN) tests were conducted on a transverse section of the welded area of sample 9 that had been etched, with a load of 500 gf applied for 15 s. S12 in the online supplementary material showed the different locations at which the microhardness tests were conducted. The indentation tests were done at 12 locations along the length of the nugget and six locations along the width of

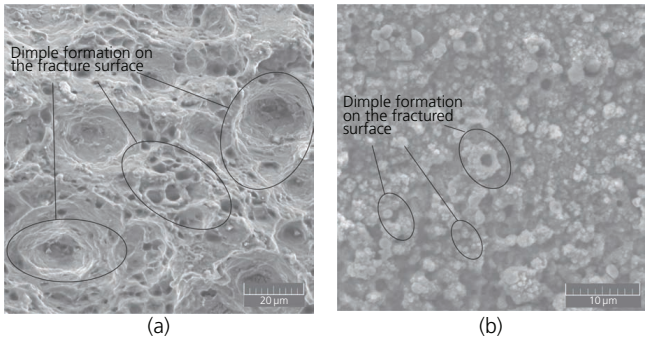

Figure 9. Fractography images of the CPT: (a) dimple formation on CPT fractured sample 6; (b) dimple formation on CPT fractured sample 9

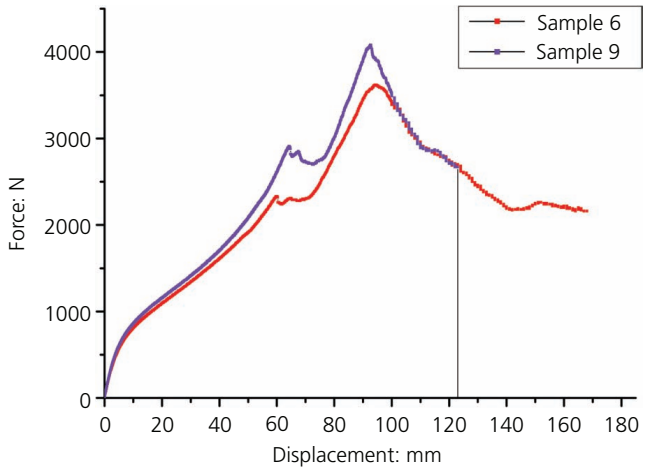

Figure 10. Load–displacement curves of the CPT

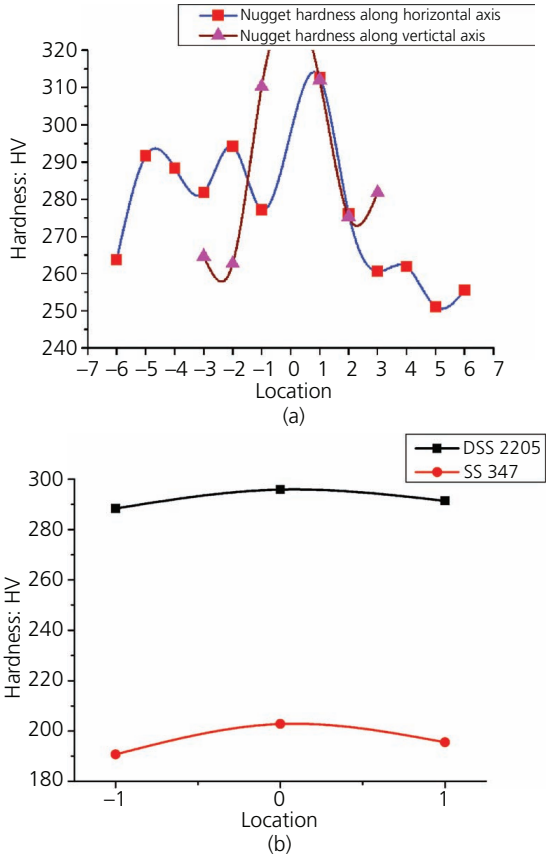

Figure 11. Hardness variation of the (a) weld nugget and (b) base metals

the nugget with a spacing of 0.5 mm between the indentations. In addition, the tests were done at three locations each on the AISI 347 and DSS 2205 base metals. Figure 11 shows the variation of the hardness of the weld nugget and the base metals. All specimens were tested in ambient air at room temperature. From the results, it is seen that the maximum hardness is recorded in the weld nugget zones, which confirms the quality of the weld properties tested in the CTT and CPT. The test results agree with the results of the microhardness testing of SS 304 weldments carried out by Kumar *et al.*[26] The distribution of the hardness values along the horizontal axis and vertical axis of the weld nugget shown in Figures 11(a) and 11(b) depicts the variation in hardness as the location is moved away from the centre of the weld nugget. The cooling rate of the weld pool plays a pivotal role in deciding the microstructural formation of the weld nugget.[27] The extremely faster cooling rates occurring during RSW cause the weld metal pool to undergo a much faster transition from the liquid phase to the ferritic phase and then to the austenitic phases. The cooling rate and the thermal conductivity of the base metals produce a combined effect on the variation of the hardness of the weld zone and the heat-affected zone. The weld solidification cycle for DSS 2205 occurs in the order of liquid metal to δ-ferrite, and then in the temperature range 1200–800°C, the phases begin to change from ferritic to austenitic, and finally cooling below 500°C results in the formation of a matrix of various ferritic and austenitic phases.[28] The air cooling occurring during the weld cycle also causes ferritic phase formation in the solidification process. The ferritic formation during the later stages of solidification cycle improves the hardness of the weld zone relative to that of the base metal. The maximum hardness is seen in the centre of the weld nugget, and the hardness is minimised gradually moving towards the heat-affected zones of the parent metals along either of the axes. The hardness values of DSS 2205 are higher than those of the AISI 347 base metal, and hence, the initial tear progresses in AISI 347, which is softer than DSS. The hardness values are maximum in the fusion zone for the chosen sample,[29] and it is found to have failed under pull-out failure mode in the CTT and CPT. This is in poor concurrence with the research conducted on the RSW of dual-phase steel sheets wherein the samples that had maximum hardness in the fusion zone failed under interfacial failure mode.[30] This contrasting behaviour of the dissimilar RSW sample exhibits the characteristics of austenitic stainless steel and DSS against the dual-phase steel sheets.

4. Conclusion

This paper focuses on analysing the failure mechanism of the dissimilar spot-welded joints of AISI 347 and DSS 2205. The mechanical properties of the weld were tested by carrying out TSTs, CTTs, CPTs and microhardness tests on samples 6 and 9. The following points were observed while investigating the fractured specimens of various tests.

- The maximum load absorbed by samples 6 and 9 during the TSTs were 16 and 18 kN, respectively. The fractography analysis of the upper and lower surfaces of sample 9 revealed that the failure was initiated through plastic deformation and finally ended with crack formation in the DSS 2205 side, resulting in a brittle pull-out failure mode.
- During the CTTs, samples 9 and 6 failed at 15.1 and 10.7 kN, respectively. Sample 6 started to fail through interfacial mode, and slowly the failure mode changed its course towards button pull-out failure, thus resulting in a partial pull-out failure mode. In contrast, sample 9 failed through pull-out failure mode. The fractography images of both samples depicted brittle fracture.
- Under CPTs, samples 9 and 6 failed at 4 and 3.6 kN, respectively. The failure mode for both samples was pull-out failure mode. The fractography analysis showed clear indications of ductile fracture through dimple formation on the surface of the fracture.
- A microhardness test was carried out at several locations along the length and width of the weld nugget and the heat-affected zones of both parent metals. The weld nugget zone recorded a maximum hardness of 312.8 HV, which was 78.74 and 7.1% higher than the base metal hardness values of AISI 347 and DSS 2205, respectively.
- The level 3 values of the welding current and heating cycles – that is, 8.5 kA and 14 cycles, resulted in a defect-free weld nugget, and these parameters could be used to obtain strong dissimilar weld joints for the AISI 347 and DSS 2205 combination.

REFERENCES

1. Sobhani S and Pouranvari M (2019) Duplex stainless steel/martensitic steel dissimilar resistance spot welding: microstructure–properties relationships. *Welding Journal* **98**: 263S–272S.
2. Arabi SH, Pouranvari M and Movahedi M (2017) Welding metallurgy of duplex stainless steel during resistance spot welding. *Welding Journal* **96**: 307s–318s.
3. Yousefian S, Zarei-Hanzaki A, Barabi A *et al.* (2021) Microstructure, texture and mechanical properties of a nickel-free high nitrogen duplex stainless steel processed through friction stir spot welding. *Journal of Materials Research and Technology* **15**: 6491–6505, https://doi.org/10.1016/j.jmrt.2021.11.040.
4. Chen L, Zhang Y, Xue X *et al.* (2022) Investigation on shearing strength of resistance spot-welded joints of dissimilar steel plates with varying welding current and time. *Journal of Materials Research and Technology* **16**: 1021–1028, https://doi.org/10.1016/j.jmrt.2021.12.079.
5. Chabok A, Cao H, van der Aa E and Pei Y (2022) New insights into the fracture behavior of advanced high strength steel resistance spot welds. *Journal of Materials Processing Technology* **301**: article 117433, https://doi.org/10.1016/j.jmatprotec.2021.117433.
6. Ding K, Wang Y, Lei M *et al.* (2022) Numerical and experimental investigations on the enhancement of the tensile shear strength for resistance spot welded TWIP steel. *Journal of Manufacturing Processes* **76**: 365378, https://doi.org/10.1016/j.jmapro.2022.02.031.
7. Rao SS, Arora KS, Sharma L and Chhibber R (2022) Modelling and optimization of resistance spot weld responses using RSM–GA technique for DP590 steel sheets. *Proceedings of the National Academy of Sciences, India Section A: Physical Sciences* **92**: 453–466, https://doi.org/10.1007/s40010-022-00772-1.
8. Zhao B, Wang Y, Ding K *et al.* (2021) Enhanced cross-tension property of the resistance spot welded medium-Mn steel by in situ microstructure tailoring. *International Journal of Steel Structures* **21**: 666–675, https://doi.org/10.1007/s13296-021-00464-3.
9. Mishra D, Rajanikanth K, Shunmugasundaram M, Kumar AP and Maneiah D (2021) Dissimilar resistance spot welding of mild steel and stainless steel metal sheets for optimum weld nugget size. *Materials Today: Proceedings* **46(Part 1)**: 919–924, https://doi.org/10.1016/j.matpr.2021.01.067.
10. Zhang Y, Guo J, Li Y, Luo Z and Zhang X (2020) A comparative study between the mechanical and microstructural properties of resistance spot welding joints among ferritic AISI 430 and austenitic AISI 304 stainless steel. *Journal of Materials Research and Technology* **9**: 574–583, https://doi.org/10.1016/j.jmrt.2019.10.086.
11. Prabhakaran M, Duraisamy J, Shanmugam NS, Kannan AR and Varatharajalu M (2023) Weld strength and microstructure analysis on resistance spot welding of austenitic AISI 347 stainless steel and duplex AISI 2205 stainless steel. *Transactions of the Indian Institute of Metals* **76(4)**: 925–936, https://doi.org/10.1007/s12666-022-02789-x.
12. Shojaee M, Midawi ARH, Barber B *et al.* (2021) Mechanical properties and failure behavior of resistance spot welded third-generation advanced high strength steels. *Journal of Manufacturing Processes* **65**: 364–372, https://doi.org/10.1016/j.jmapro.2021.03.047.
13. Ramasamy N, Jeyasimman D and Raju N (2020) Effect of intermetallic compounds and inclusions in normalizing rolled C–Mn steel plate butt joint failure. *Transactions of the Indian Institute of Metals* **73(9)**: 2333–2343, https://doi.org/10.1007/s12666-020-02038-z.
14. Ramasamy N, Jeyasimman D, Kathiravan R and Raju N (2019) Influence of welding sequence on residual stresses induced in as-welded plug weld of low-carbon steel plate. *Transactions of the Indian Institute of Metals* **72(5)**: 1361–1369, https://doi.org/10.1007/s12666-019-01631-1.
15. Pandya KS, Grolleau V, Roth CC and Mohr D (2020) Fracture response of resistance spot welded dual phase steel sheets: experiments and modeling. *International Journal of Mechanical Sciences* **187**: article 105869, https://doi.org/10.1016/j.ijmecsci.2020.105869.
16. Bhuvaneswaran S and Padmanaban R (2021) Prediction of spot weld fatigue life using finite element approach. *Materials Today: Proceedings* **46(Part 19)**: 9875–9881, https://doi.org/10.1016/j.matpr.2020.12.816.
17. Onar V (2022) Mechanical and microstructural characterizations of resistance spot welded dissimilar TWIP/304L stainless steel. *Transactions of the Indian Institute of Metals* **75(7)**: 1731–1739, https://doi.org/10.1007/s12666-021-02446-9.
18. Taufiqurrahman I, Ahmad A, Mustapha M *et al.* (2021) The effect of welding current and electrode force on the heat input, weld diameter, and physical and mechanical properties of SS316l/Ti6Al4V dissimilar resistance spot welding with aluminum interlayer. *Materials* **14(5)**: article 1129, https://doi.org/10.3390/ma14051129.
19. Wang B, Qiu F, Chen L *et al.* (2022) Microstructure and shearing strength of stainless steel/low carbon steel joints produced by resistance spot welding. *Journal of Materials Research and Technology* **20**: 2668–2679, https://doi.org/10.1016/j.jmrt.2022.08.041.
20. Pouranvari M (2012) Susceptibility to interfacial failure mode in similar and dissimilar resistance spot welds of DP600 dual phase steel

and low carbon steel during cross-tension and tensile–shear loading conditions. *Materials Science and Engineering: A* **546**: 129–138, https://doi.org/10.1016/j.msea.2012.03.040.

21. Chen N, Wang HP, Carlson BE, Sigler DR and Wang M (2018) Fracture mechanisms of Al/steel resistance spot welds in coach peel and cross tension testing. *Journal of Materials Processing Technology* **252**: 348–361, https://doi.org/10.1016/j.jmatprotec.2017.09.035.
22. Rao SS, Arora KS, Sharma L and Chhibber R (2021) Investigations on mechanical behaviour and failure mechanism of resistance spot-welded DP590 steel using artificial neural network. *Transactions of the Indian Institute of Metals* **74(6)**: 1419–1438, https://doi.org/10.1007/s12666-021-02237-2.
23. Marashi P, Pouranvari M, Sanaee SMH *et al.* (2008) Relationship between failure behaviour and weld fusion zone attributes of austenitic stainless steel resistance spot welds. *Materials Science and Technology* **24(12)**: 1506–1512, https://doi.org/10.1179/174328408X262418.
24. Arumugam A and Pramanik A (2022) A study of spot weld pull-out failure (PF) mechanism under different loading conditions for stainless steel and mild steel joints. *Australian Journal of Mechanical Engineering* **20(3)**: 603–616, https://doi.org/10.1080/14484846.2020.1725348.
25. ASTM (2017) ASTM E384: Standard test method for microindentation hardness of materials. ASTM, West Conshohocken, PA, USA.
26. Kumar R, Chohan JS, Goyal R and Chauhan P (2020) Impact of process parameters of resistance spot welding on mechanical properties and micro hardness of stainless steel 304 weldments. *International Journal of Structural Integrity* **12(3)**: 366–377, https://doi.org/10.1108/IJSI-03-2020-0031.
27. Nhung LT, Khanh PM, Hai LM and Nam ND (2017) The relationship between continuous cooling rate and microstructure in the heat affected zone (HAZ) of the dissimilar weld between carbon steel and austenitic stainless steel. *Acta Metallurgica Slovaca* **23(4)**: 363–370, https://doi.org/10.12776/ams.v23i4.1002.
28. Verma J and Taiwade RV (2017) Effect of welding processes and conditions on the microstructure, mechanical properties and corrosion resistance of duplex stainless steel weldments – a review. *Journal of Manufacturing Processes* **25**: 134–152, https://doi.org/10.1016/j.jmapro.2016.11.003.
29. Mohammed HG, Ginta TL and Mustapha M (2020) The investigation of microstructure and mechanical properties of resistance spot welded AISI 316L austenitic stainless steel. *Materials Today: Proceedings* **46(Part 4)**: 1640–1644, https://doi.org/10.1016/j.matpr.2020.07.258.
30. Đurić A, Milčić D, Marković B *et al.* (2021) Resistance spot welding of steel sheet DP500 – influence of the welding current on the microhardness and weld nugget diameter. *Proceedings of the 11th International Scientific-Professional Conference (SBW 2021), Slavonski Brod, Croatia*, pp. 27–30.